Title
Development of a broadband reflectivity diagnostic for laser driven shock compression experiments

Journal
Review of Scientific Instruments, 86(4)

ISSN
0034-6748

Authors
Ali, SJ
Bolme, CA
Collins, GW
et al.

Publication Date
2015-04-01

DOI
10.1063/1.4917195

Peer reviewed

AIP | Review of Scientific Instruments

Development of a broadband reflectivity diagnostic for laser driven shock compression experiments

S. J. Ali, C. A. Bolme, G. W. Collins, and R. Jeanloz

Citation: Review of Scientific Instruments **86**, 043112 (2015); doi: 10.1063/1.4917195
View online: http://dx.doi.org/10.1063/1.4917195
View Table of Contents: http://scitation.aip.org/content/aip/journal/rsi/86/4?ver=pdfcov
Published by the AIP Publishing

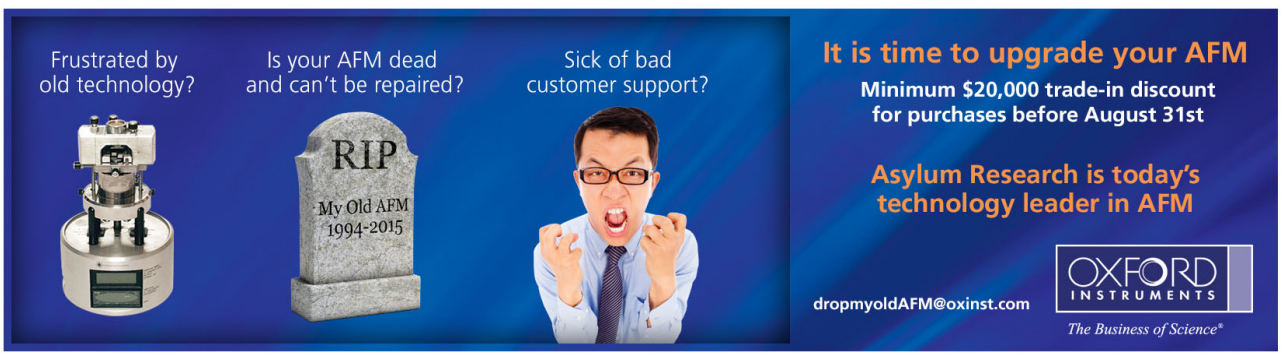

Development of a broadband reflectivity diagnostic for laser driven shock compression experiments

S. J. Ali,[1,2] C. A. Bolme,[3] G. W. Collins,[2] and R. Jeanloz[4]
[1]*Department of Chemistry, University of California, Berkeley, California 94720, USA*
[2]*Lawrence Livermore National Laboratory, 7000 East Ave., Livermore, California 94550, USA*
[3]*Shock and Detonation Physics, Los Alamos National Laboratory, Los Alamos, New Mexico 87545, USA*
[4]*Department of Earth and Planetary Science, University of California, Berkeley, California 94720, USA*

(Received 13 September 2014; accepted 28 March 2015; published online 16 April 2015)

A normal-incidence visible and near-infrared shock wave optical reflectivity diagnostic was constructed to investigate changes in the optical properties of materials under dynamic laser compression. Documenting wavelength- and time-dependent changes in the optical properties of laser-shock compressed samples has been difficult, primarily due to the small sample sizes and short time scales involved, but we succeeded in doing so by broadening a series of time delayed 800-nm pulses from an ultrafast Ti:sapphire laser to generate high-intensity broadband light at nanosecond time scales. This diagnostic was demonstrated over the wavelength range 450–1150 nm with up to 16 time displaced spectra during a single shock experiment. Simultaneous off-normal incidence velocity interferometry (velocity interferometer system for any reflector) characterized the sample under laser-compression and also provided an independent reflectivity measurement at 532 nm wavelength. The shock-driven semiconductor-to-metallic transition in germanium was documented by the way of reflectivity measurements with 0.5 ns time resolution and a wavelength resolution of 10 nm. © *2015 AIP Publishing LLC.* [http://dx.doi.org/10.1063/1.4917195]

I. INTRODUCTION

Materials undergoing dynamic compression, whether with shock, multi-shock, or ramp loading, can exhibit dramatic changes in physical and chemical properties that are evident in the optical properties of the sample. Measurement of sample reflectivity is vital for characterizing changes in chemical bonding, and the associated electronic structure, of materials.[1–7] Although current diagnostics are sufficient for many Hugoniot measurements,[8,9] documenting time- and wavelength-dependent optical properties remains a challenge. Velocimetry does provide kinematic information, but requires significant volume changes in order to indicate phase changes or chemical reactions, and is often incapable of distinguishing important changes in the electronic structure of the sample. Single channel pyrometry across the visible wavelengths is also frequently used to estimate the temperature of shocked materials and in tandem with velocimetry can provide more detailed information about the material's path through pressure-temperature space, but the single-channel nature of the diagnostic and frequent grey-body assumption of the material's emissivity often results in large potential errors due to uncertain wavelength-dependent emissivity.[10,11] While an acceptable assumption for many experiments, if the shocked material undergoes any changes in optical properties or if the emissivity of the material has any wavelength dependence, measurement of thermal emission does not accurately represent temperature of the sample. Recent publications highlight the need for broadband reflectivity measurements as a means of determining the wavelength-dependent emissivity of shock-compressed metals and, in part, dielectrics.[10,11]

X-ray diffraction of shock compressed materials can provide an unequivocal identification of phase transitions, as it probes the local material order; however, it is rarely able to provide information on chemistry and can be difficult to use on amorphous or liquid materials. Spectroscopy provides much of our understanding of chemical and physical properties at ambient conditions, yet it has—until recently—proven too challenging for use with laser-induced compression. This lack of diagnostic capability is predominately a result of the inherent difficulty in attempting to observe optical changes in materials under conditions of extreme pressure, a difficulty primarily related to the nanosecond temporal scales and micron-to-millimeter sample sizes of interest. A nanosecond pulse duration laser drive propagates a shock wave through a target material over the course of nanoseconds, excluding the use of many common spectrophotometric techniques, as these techniques utilize low intensity light sources or alternatively scan through the desired wavelengths using a rotating grating monochrometer.[12] In order to address the temporal and spatial constraints mentioned above, researchers have tended toward two approaches. Interesting work has been done developing broadband optical spectroscopy diagnostics for use on gas gun and explosively driven experiments, which utilize millimeter-to-centimeter sample sizes and time scales on the order of microseconds.[13–18] While these experiments provide a great deal of information on material properties under compression, the large sample sizes and lower temporal resolution can limit the visibility of faster property changes, such as chemical reactions. The high photon intensities and broad spectral range required for data collection over short time-scales can be obtained using broadening of an ultra-fast laser in a dielectric

medium, a method developed over the past 40 years.[19–21] Using this broadening technique, a considerable amount of work has been done in the last decade developing transient absorption spectroscopy of laser driven shock compressed samples.[22–27] This has provided a great deal of insight into the chemical changes accompanying compression; however, the measurements are limited to a single time point per shot and therefore does not probe time-dependent spectral changes.

Building on the aforementioned work, we have developed a diagnostic system that allows us to measure the optical properties of laser-compressed materials over nanosecond time scales at visible and near-infrared (NIR) wavelengths. The requisite high-intensity white light was produced via supercontinuum generation in a non-linear optical medium and sub-nanosecond time resolution was achieved using an optical pulse stacker. Using this diagnostic, we documented a two-fold increase in reflectivity for shock-compressed germanium as it transformed from the ambient diamond structure to a more metallic structure, most likely the β-Sn structure that has been observed in static diamond-anvil cell experiments.[3,28]

II. EXPERIMENTAL TECHNIQUE

A. Shock generation and velocimetry

The overall goal of the diagnostic system was to simultaneously measure broadband reflectivity and collect velocimetry data using a Velocity Interferometer System for Any Reflector (VISAR) from the surface of a target undergoing shock compression.[8,9] The experiment that follows was conducted using the two-beam Nd:glass Janus laser system operated by the Jupiter Laser Facility in Lawrence Livermore National Laboratory. The target design for these experiments (Fig. 1) consisted of a reflective germanium sample with a parylene-coated aluminum pusher on the drive side and a transparent lithium fluoride window on the diagnostic side.

The target was placed in the vacuum chamber (center left of Fig. 2). A 40-400 J laser pulse was used to generate a high pressure compression wave in the sample, with the peak pressure depending on the energy deposited from the laser. A 1-mm-square phase plate and a 6-ns-square pulse were used for the experiments presented. The compression

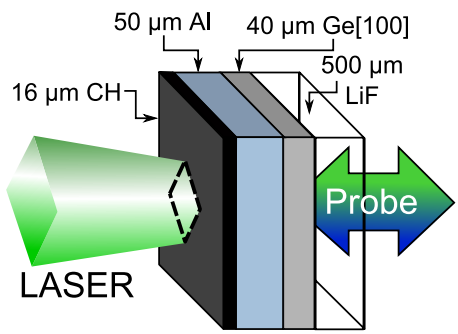

FIG. 1. Target design for the discussed experiments. The material of interest, in this case germanium, was sandwiched between a lithium fluoride window to prevent spall and an aluminum pusher with an ablative plastic layer on the drive side.

wave steepened into a shock wave and propagated through the sample; this compression resulted in structural and electronic changes in the target material, the nature of which could be probed using the shock wave optical reflectivity diagnostic (SWORD). Information about the pressure and density of the sample was obtained using the aforementioned VISAR. A pulsed 532-nm Nd:YAG laser was used for the VISAR probe and reflected from the surface of the sample at a 27° angle from normal and collected at 27° using an f/3 imaging system with a focal length of 14.6 cm.[29] The velocimetry data were corrected for the off-normal angle of incidence as described by Dolan.[30]

B. Broadband reflectivity

A Coherent HIDRA pumped by a Continuum PowerLite 8000 was used as the ultrafast laser source for the broadband reflectivity diagnostic, providing 20-25 mJ of energy at 800 nm with variable pulse duration between 50 fs and 100 fs. As shown in the upper right side of Figure 2, the collimated ultrafast pulse was stacked in time using a series of adjustable time delay paths. The temporal delay provided by the differing path lengths allowed for a degree of time resolution, as well as the ability to collect multiple spectra over the course of a single shock compression experiment. The ultrafast pulse was directed through a series of 50:50 beamsplitters (CVI BTF-NIR-50-SQW-5001M-C), each of which directed approximately half of the beam intensity into an air delay path of known length. Each subsequent beamsplitter also served to recombine the delayed pulse such that it was collinear with the zero delay beam path. Four beamsplitters and four delay paths were used to generate 16 pulses. A pulse-to-pulse time interval of 0.5 ns was used for the experiment, with delay path lengths set to 15 cm, 30 cm, 60 cm, and 120 cm (0.5 ns, 1 ns, 2 ns, and 4 ns). As the reflection/transmission ratio of the beamsplitters was dependent on beam polarization, half-waveplates were installed in two of the delay paths, as well as immediately prior to the pulse stacker. In order to obtain equal intensities for all 16 pulses, it was necessary to iteratively adjust the rotation of the three half-waveplates while observing the pulse intensities on a streak camera. The spectral broadening process discussed below was highly nonlinear; relatively small differences in the pulse intensities across the 16 pulses would be amplified, often resulting in a loss of intensity at wavelengths further from the fundamental.[19] Although it would have precluded the complicated referencing procedure discussed below, due to the difficulty in obtaining 50:50 beamsplitters and half-waveplates with a working range that encompassed the entire wavelength range produced in the broadened beam, it was determined that the pulse stacking must occur before the ultrafast pulse was broadened. This location for the pulse stacking also had the added benefit of lowering the beam power that was focused into the optically nonlinear medium for broadening, reducing the likelihood of damaging the material or any optics handling the reduced beam diameter.

The stacked collimated pulses were focused using a 500-mm achromat into a 1-cm-long water cell, wherein a set of nonlinear optical processes, most importantly self-focusing and self-phase modulation, result in a broadened spectrum

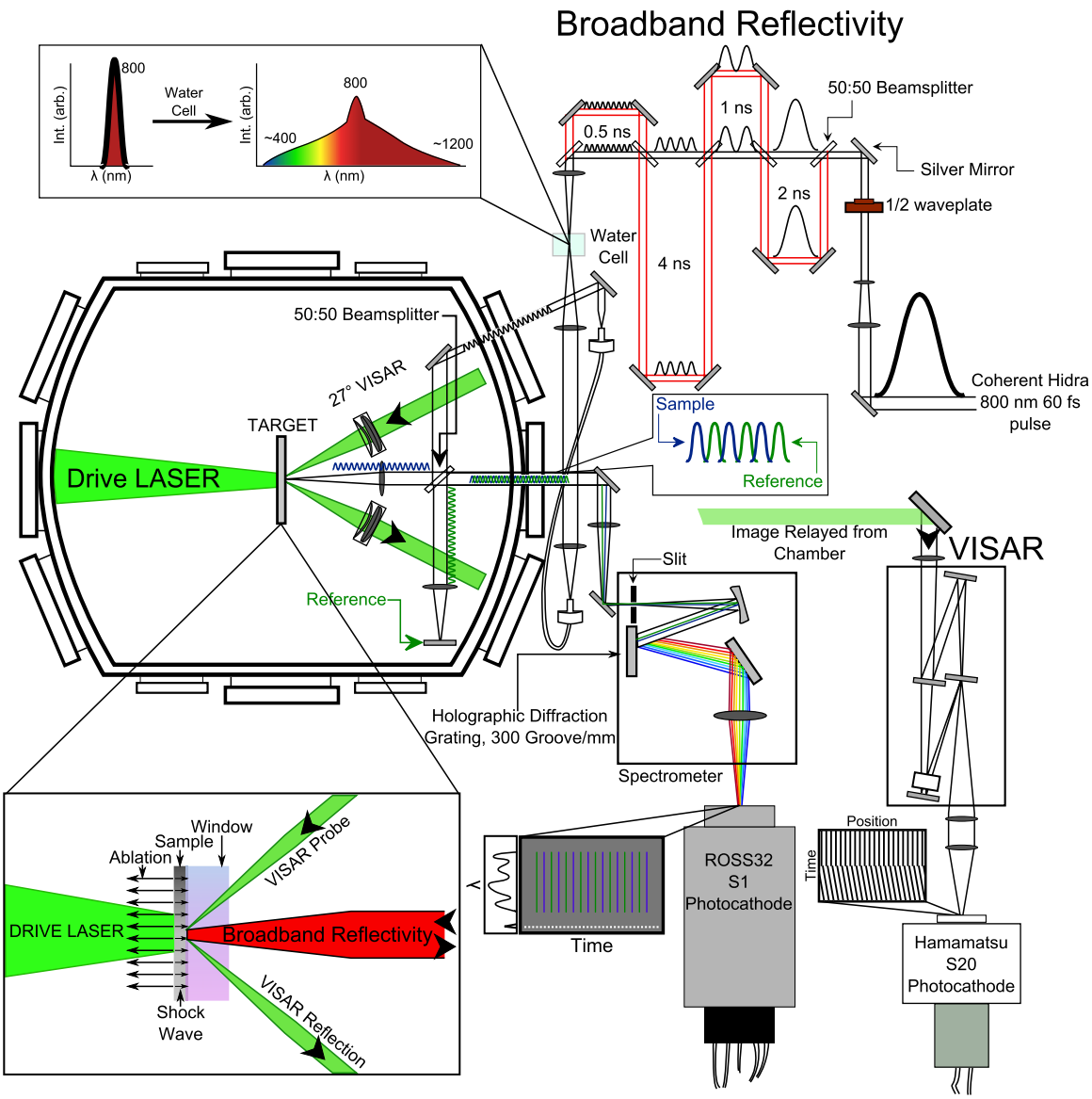

FIG. 2. Optical schematic of the broadband reflectivity system with target inset in the bottom left. The ultrafast pulse entered the pulse stacking system outlined in the upper right corner. The stacked pulses were focused into the water cell which generated wavelength broadened light as shown in the upper left corner. The sample and reference pulses from the target chamber were collected in a spectrometer and swept in time on the ROSS streak camera. The VISAR 532 nm probe beam entered the chamber and was directed to the target at a 27° angle and collected at −27° by an identical set of imaging optics. The optical path from the chamber to the VISAR interferometer was not shown due to space constraints. A full schematic of the VISAR optical setup can be found in Ref. 29.

of approximately 400–1200 nm, as shown in Figure 3.[21,31–34] As mentioned above, the spectral broadening in the dielectric material is highly nonlinear in its dependence on the laser intensity,[21,32,34,35] requiring the generation of independent spectral references for each of the time delayed pulses, as will be discussed in more detail below.

The white light was collimated using a 500-mm achromat and, after passing through a notch filter to remove the excess fundamental laser light at 800 nm, injected into a 1-m-long 200-μm-diameter core high-damage threshold fiber using a 40× microscope objective. Injection into a fiber served two important purposes: the first was to spatially homogenize the broadened light and the second was to effectively decouple the sensitive alignment of the pulse stacker from the alignment to the target and the detector. The illumination from the fiber was collected immediately outside the vacuum chamber, collimated to a 3.8-cm-diameter, and directed through a broadband antireflection-coated chamber window. Within the chamber, the broadened light was passed through a 45° beamsplitter with 50% ± 5% transmission in the wavelength range of interest (Edmund Optics 45-854 in the visible, 45-855 in the near-infrared). At the beamsplitter, the reflected light was directed toward the target and the transmitted light was directed toward a static reference. Both beams were independently focused onto their respective surfaces using matching f/4.5 imaging systems with a focal length of 15 cm. The reflected light was recombined at the original beamsplitter with a 0.25-ns delay between each sample and reference pulse arising from the 7.5-cm path-length difference between the two beam paths. The light from the sample and reference was focused using a 50-mm focal length achromat into a home built spectrometer with a low wavelength dispersion that enabled the detector to

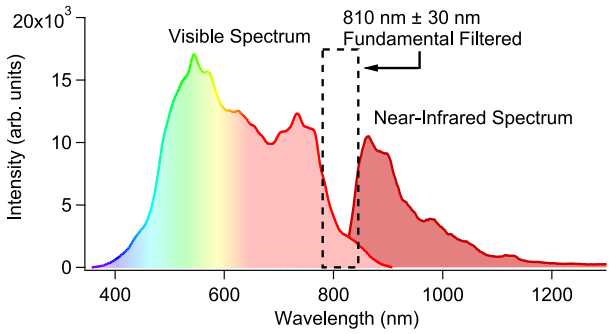

FIG. 3. Representative spectra generated using the white light supercontinuum generation in a 1 cm water cell. A filter was used to attenuate the remaining fundamental light centered at 810 nm.

capture either the full visible range or the near infrared from 800 to 1200 nm. The spectrometer output was imaged on a Rochester Optical Streak System (ROSS) camera with a sweep window of 16 ns. The ROSS camera used an S1 photocathode with efficiency between 20% and 85% in the wavelength range 400-1600 nm, allowing reflectivity measurements across the visible and near-infrared.[36–38]

Alignment of the VISAR probe, reflectivity probe, and drive laser was accomplished employing a target consisting of a 250-μm transparent square of quartz with a ~200 nm coating of aluminum into which a cross had been etched. The three beam paths were co-aligned to this etched cross, ensuring that the diagnostics were observing the center of the laser shocked region.

The raw data consist of an interleaved set of 16 sample pulses and 16 reference pulses. A characteristic set of raw data can be seen in Figure 4(a), with false color emphasizing the difference between the sample and reference pulses. A series of 10-20 images were taken prior to the shock compression to obtain the scaling factor accounting for the difference between the reference and sample optical paths.

C. Analysis

The analysis consisted of two parts: the first was the extraction of the spectra from the streak camera records and the second was the scaling and normalization of those spectra relative to a standard. As can be seen in Figure 4(a), due to a combination of factors including spectral chirp and a small degree of nonlinearity in the streak tube and CCD, the spectra were neither parallel nor of equal width across the wavelength axis. To determine the location of each reflected pulse on the image, a series of equally spaced vertical line outs were taken and the minima were located; each local minimum indicated the termination of one pulse and the beginning of the next. The final spectra were obtained by integrating each column of pixels in the temporal dimension between the minima locations. The results of such integration can be seen in Figure 4(b).

This extraction process was applied to the static reference images in order to obtain a scaling factor accounting for the slight optical path difference between the pulses reflecting from the sample surface and those reflecting from the reference

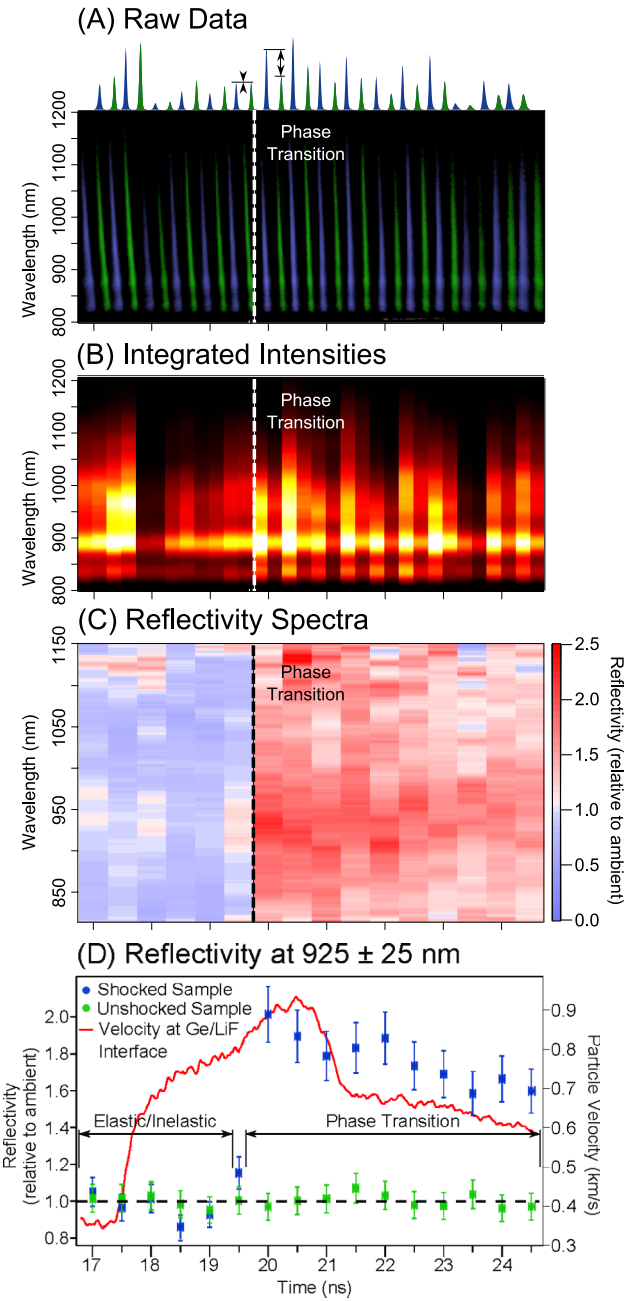

FIG. 4. (a) Raw data from the broadband reflectivity diagnostic. False color has been used for clarity; the 16 blue pulses are sample pulses and the 16 green pulses are reference pulses, following the schematic in Figure 2. The time scale shown was relative to the arrival of the drive laser pulse. (b) Integrated intensities extracted from the raw data in (a). The aforementioned increase in the intensity of the sample pulses relative to the static reference pulses can be observed at 19.5 ns. (c) Reflectivity spectra obtained by comparing the sample intensities to the static reference intensities in (b). Following elastic wave arrival at 15 ns and inelastic wave arrival at 17.5 ns, there was a small decrease (5%-10%) in the intensity of the sample pulses, most likely due to a slight roughening of the target surface. An 80%-90% increase in the reflectivity of the germanium sample was observed at 19.5 ns, which indicates the germanium phase transition accompanied by closure of the band gap. (d) Reflectivity between 900 and 950 nm extracted from (c). The small decrease in reflectivity that accompanied the elastic and inelastic precursors can be observed between 17 and 19 ns, with the significant increase that accompanied the phase transition beginning at 19.5 ns. The dashed black line at a reflectivity of one is a guide for the eye. The red line is particle velocity at the germanium-LiF interface obtained from the VISAR. The elastic wave begins prior to the SWORD time window, but rise of the inelastic wave can be seen at 17.5 ns and the arrival of a phase transition wave can be observed at 19.5 ns.

surface. This scaling factor was determined for each target and the resolution limit of the diagnostic was determined by applying this scaling factor to unshocked images and observing the deviation from an ideal value of one. For a series of images taken using an unshocked target, any series of scaling factors obtained using one image should be identical to those obtained using another image of the same target and any deviation from identicalness was indicative of systematic errors in the instrumentation.

The final spectra were obtained by extraction from the image and then scaling to account for optical path differences between the sample and reference. An example of shocked spectra can be seen in Figure 4(c). The sharp, almost two-fold increase in near-infrared reflectivity that occurred between 19.5 and 20 ns can be seen more clearly in Figure 4(d), which shows lineouts in time taken between 900 and 950 nm from Figure 4(c).

III. RESULTS AND DISCUSSION

In order to test this new broadband reflectivity diagnostic, a series of laser-shock experiments were conducted on single crystal germanium in the target configuration shown in Figure 1. Germanium has previously been shown to go through a phase transition at ~10 GPa under static compression, from a diamond-like semiconductor to a β-Sn semi-metal.[2,39–42] A significant increase in electrical conductivity, and therefore reflectivity, is expected at this transition in Ge, from a structure with a more covalent to a more metallic bonding character.[43,44] Previous static experiments also indicate a degree of wavelength dependence in this reflectivity increase, which might potentially be observed using the broadband reflectivity diagnostic.[45] The most significant change in the reflectivity of germanium under pressure, as observed by Hanfland *et al.*, occurs in the NIR, with the increase ranging from 130% to 200% between 800 and 1200 nm for the 13.6-GPa compression and 140%–200% for the 34.4-GPa compression. Changes in the visible reflectivity were also observed; however, the magnitude of the reflectivity increase is less significant and peaks at 156% at 425 nm. Initial experiments were designed to test the feasibility of the SWORD and, as such, reflectivity spectra were taken primarily in the NIR. Following the success of these early experiments, later experiments obtained data spanning wavelength ranges from the visible to the NIR, as can be observed in Figure 5.

Figure 5 compares data from two different shots at varying peak pressures with static compression data from Hanfland *et al.* The spectrometer was shifted such that the observed wavelength range was 550 nm–900 nm. As was seen previously, we observe a high metallic-like reflectivity in the NIR which decreases in the visible. Features in the visible are most likely due to interband transitions and are consistent with a nearly free-electron metal as would be expected from germanium in the β-Sn phase. In comparison to primarily static compression literature data, caution must be used due to the temperature and strain rate differences, but there is agreement between our data and the optical reflection data from Hanfland *et al.*

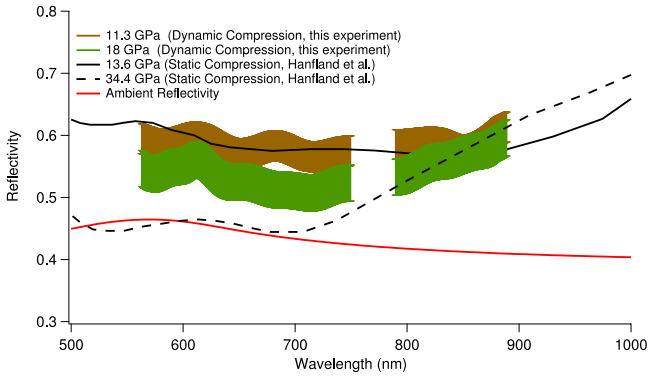

FIG. 5. Normalized reflectivity from this experiment and Hanfland *et al.* The gap between 750 nm and 790 nm is a result of filtering to remove a 780 nm fundamental peak. Both lineouts were taken at the peak of the phase transition wave.

IV. CONCLUSIONS

A new diagnostic has been developed in order to probe the optical properties of materials compressed to high pressures and temperatures using laser-driven compression. The SWORD provides broadband reflectivity across visible and near-infrared wavelengths with a spectral resolution of 10 nm and a time resolution as low as 0.5 ns. This diagnostic will allow for the characterization of changes in the optical properties of highly compressed materials and the emissivity information obtained from this diagnostic will greatly improve the precision of existing pyrometric diagnostics.[10]

ACKNOWLEDGMENTS

S.J.A. is funded through the Livermore Graduate Scholars Program. The researchers would like to thank technical staff at the Jupiter Laser Facility for invaluable support in conducting this experiment and J. Eggert, R. Smith, and P. Celliers for advice with regards to data analysis. This work was performed under the auspices of the U.S. Department of Energy by Lawrence Livermore National Laboratory under Contract No. DE-AC52-07NA27344.

[1]R. Zallen and W. Paul, "Band structure of gallium phosphide from optical experiments at high pressure," Phys. Rev. A **134**(6A), 1628 (1964).
[2]S. Minomura and H. G. Drickamer, "Pressure induced phase transitions in silicon, germanium and some 3-5 compounds," J. Phys. Chem. Solids **23**, 451 (1962).
[3]R. J. Nelmes *et al.*, "Structural studies of Iii-V and group-Iv semiconductors at high-pressure," J. Phys. Chem. Solids **56**(3-4), 539–543 (1995).
[4]N. J. Trappeniers and R. Vetter, "High-resolution measurement of germanium absorption-edge under pressure," Physica **60**(1), 235 (1972).
[5]W. Paul, "Band structure of Intermetallic semiconductors from pressure experiments," J. Appl. Phys. **32**, 2082 (1961).
[6]H. Abid *et al.*, "Pressure-dependence of band-gaps in Gaas, Gap, Inp, and Inas," Mater. Chem. Phys. **38**(2), 162–168 (1994).
[7]P. Harris, "Band-gap collapse in uniaxially strained (shocked) elastic germanium," J. Appl. Phys. **51**(11), 6033–6034 (1980).
[8]L. M. Barker and R. E. Hollenbach, "Laser interferometer for measuring high velocities of any reflecting surface," J. Appl. Phys. **43**(11), 4669 (1972).
[9]L. M. Barker and R. E. Hollenbach, "Shock-wave study of alpha reversible epsilon-phase transition in iron," J. Appl. Phys. **45**(11), 4872–4881 (1974).
[10]D. K. Spaulding *et al.*, "New optical diagnostics for equation of state experiments on the Janus laser," AIP Conf. Proc. **955**, 1071–1074 (2007).
[11]B. Svendsen, J. D. Bass, and T. J. Ahrens, "Optical radiation from shock-compressed materials and interfaces," Phy. Rep. **180**(6), 333–416 (1989).

[12]W. Demtröder, *Laser Spectroscopy* (Springer, 2002).
[13]G. D. Stevens *et al.*, "Reflectance changes during shock-induced phase transformations in metals," Rev. Sci. Instrum. **81**(6), 065101 (2010).
[14]G. D. Stevens *et al.*, "Optical response of cerium-doped lutetium oxyorthosilicate coatings at shocked surfaces," Rev. Sci. Instrum. **75**(2), 462–466 (2004).
[15]A. Seifter *et al.*, "Emissivity measurements of shocked tin using a multiwavelength integrating sphere," J. Appl. Phys. **110**(9), 093508 (2011).
[16]W. D. Turley *et al.*, "Infrared emissivity of tin upon release of a 25 GPa shock into a lithium fluoride window," J. Appl. Phys. **110**(10), 103510 (2011).
[17]B. M. La Lone *et al.*, "Release path temperatures of shock-compressed tin from dynamic reflectance and radiance measurements," J. Appl. Phys. **114**(6), 063506 (2013).
[18]D. H. Dolan, T. Ao, and C. T. Seagle, "Reflectance thermometry in dynamic compression experiments," AIP Conf. Proc. **1552**, 767–770 (2013).
[19]R. R. Alfano, "The supercontinuum gains momentum," Laser Focus World **41**(5), 83–86 (2005).
[20]R. R. Alfano and S. L. Shapiro, "Continuous emission in region 4000 to 7000 a via 4-Photon coupling in glass," Phys. Rev. Lett. **24**, 584 (1970).
[21]R. R. Alfano and S. L. Shapiro, "Observation of self-phase modulation and small-scale filaments in crystals and glasses," Phys. Rev. Lett. **24**(11), 592 (1970).
[22]S. D. McGrane, D. S. Moore, and D. J. Funk, "Ultrafast spectroscopy and interferometry of laser shocked thin films: Practical considerations," Proc. SPIE **5448**, 165–170 (2004).
[23]D. S. Moore, S. D. McGrane, and D. J. Funk, "Ultrafast infrared absorption and dynamic ellipsometry of shock-compressed energetic materials," Abstracts of Papers of the American Chemical Society **227**, U316–U316 (2004).
[24]S. D. McGrane *et al.*, "Molecular shock response of Explosives: Electronic absorption spectroscopy," AIP Conf. Proc. **1195**, 1301–1304 (2009).
[25]S. D. McGrane *et al.*, "Ultrafast dynamic ellipsometry and spectroscopy of laser shocked materials," AIP Conf. Proc. **1278**, 392–400 (2010).
[26]K. E. Brown *et al.*, "Ultrafast chemical reactions in shocked nitromethane probed with dynamic ellipsometry and transient absorption spectroscopy," J. Phys. Chem. A **118**(14), 2559–2567 (2014).
[27]N. C. Dang *et al.*, "Shock induced chemistry in liquids studied with ultrafast dynamic ellipsometry and visible transient absorption spectroscopy," J. Phys. Chem. A **116**(42), 10301–10309 (2012).
[28]R. J. Nelmes *et al.*, "Imma phase of germanium at similar to 80 GPa," Phys. Rev. B **53**(6), R2907-R2909 (1996).
[29]P. M. Celliers *et al.*, "Line-imaging velocimeter for shock diagnostics at the OMEGA laser facility," Rev. Sci. Instrum. **75**(11), 4916 (2004).
[30]D. H. Dolan, Foundations of VISAR Analysis, in Sandia Report2006, Sandia National Laboratories.
[31]J. T. Manassah, R. R. Alfano, and M. Mustafa, "Spectral distribution of an ultrafast supercontinuum laser source," Phys. Lett. A **107**(7), 305–309 (1985).
[32]J. T. Manassah *et al.*, "Ultrafast supercontinuum laser source," Photonics Spectra **18**(11), 53 (1984).
[33]J. T. Manassah *et al.*, "Induced supercontinuum and steepening of an ultrafast laser-pulse," Phys. Lett. A **113**(5), 242–247 (1985).
[34]J. T. Manassah *et al.*, "Spectral extent and pulse shape of the supercontinuum for ultrashort laser-pulse," IEEE J. Quantum Electron. **22**(1), 197–204 (1986).
[35]R. R. Alfano and S. L. Shapiro, "Emission in region 4000 to 7000 a via 4-photon coupling in glass," Phys. Rev. Lett. **24**(11), 584 (1970).
[36]F. Gex *et al.*, "S1-photocathode image converter tubes," in *Proceedings of the Society of Photo-Optical Instrumentation Engineers* (P Soc Photo-Opt Inst, 1985), Vol. 491, pp. 276–280.
[37]P. A. Jaanimagi *et al.*, "The streak camera development program at LLE," *26th International Congress on High Speed Photography and Photonics* (P Soc Photo-Opt Inst, 2005), Vol. 5580, pp. 408–415.
[38]R. J. Brooks *et al.*, "Experimental data on the reflection and transmission spectral response of photocathodes," Proc. SPIE **6660**, 66013 (2007).
[39]M. Hebbache, "Elastic phase-transition in germanium and silicon," Phys. Rev. B **49**(10), 6522–6527 (1994).
[40]R. A. Graham, O. E. Jones, and J. R. Holland, "Physical behavior of germanium under shock wave compression," J. Phys. Chem. Solids **27**(9), 1519 (1966).
[41]R. A. Graham, O. E. Jones, and J. R. Holland, "Shock-wave compression of germanium from 20 to 140 Kbar," J. Appl. Phys. **36**(12), 3955 (1965).
[42]W. H. Gust and E. B. Royce, "Axial yield strengths and phase-transition stresses for (100), (110), and (111) germanium," J. Appl. Phys. **43**(11), 4437 (1972).
[43]M. Baldini *et al.*, "High-pressure EXAFS measurements of crystalline Ge using nanocrystalline diamond anvils," Phys. Rev. B **84**(1), 014111 (2011).
[44]J. M. D. Lane and A. P. Thompson, "Molecular dynamics simulation of shock-induced phase transition in germanium," AIP Conf. Proc. **1195**, 1157–1160 (2009).
[45]M. Hanfland *et al.*, "Optical-Properties of high-pressure metallic phases of Si and Ge," Semicond. Sci. Technol. **4**(4), 250–251 (1989).